Available online at www.sciencedirect.com
ScienceDirect
Journal of Photochemistry and Photobiology A: Chemistry 193 (2008) 56–64
Journal of Photochemistry and Photobiology A:Chemistry
www.elsevier.com/locate/jphotochem

# Photochemical selective deposition of nickel using a $TiO_2$–$Pd^{2+}$ layer

T.V. Byk [a,*], V.G. Sokolov [b], T.V. Gaevskaya [b], E.V. Skorb [b], D.V. Sviridov [b], Chang-Ho Noh [a], Ki Yong Song [a], Young Nam Kwon [a], Sung Hen Cho [a]

[a] *Samsung Advanced Institute of Technology, P.O. Box 111, Suwon 440-600, Republic of Korea*
[b] *Research Institute for Physical and Chemical Problems of the Belarusian State University, Leningradskaya 14, Minsk 220050, Belarus*

Received 19 September 2006; received in revised form 9 April 2007; accepted 11 June 2007
Available online 14 June 2007

**Abstract**

The mechanism of photochemical selective deposition of nickel employing an amorphous $TiO_2$–$Pd^{2+}$ layer with entrapped oxalic acid as a sensitizer has been studied by X-ray photoelectron spectroscopy, FT-IR spectroscopy, and TEM, SEM and AFM analyses. Exposure of $TiO_2$–$Pd^{2+}$ layers to UV light is believed to yield predominantly Pd(I) compounds stabilized in a photopolymerized matrix of titanium oxide. These compounds are capable of undergoing disproportionation during washing, which results in completion of Pd nanophase formation at the exposed areas. Increasing the UV light intensity from 8 to 30 mW $cm^{-2}$ affects the structure and size of the obtained Pd particles and their catalytic activity towards nickel electroless plating. As a result, both negative and positive patterns can be obtained employing the same $TiO_2$–$Pd^{2+}$ photolayers.


*Keywords:* Photochemical selective nickel deposition; Amorphous titanium oxide; Palladium; Oxalic acid

## 1. Introduction

Titanium dioxide is the most investigated semiconductor catalyst for applied photocatalysis [1–3]. Photochemical processes using $TiO_2$ as a heterogeneous catalyst involve absorption of supra-bandgap photons generating photoexcited electrons ($e^-$) and holes ($h^+$). The photoelectrons and holes may diffuse to the surface of the semiconductor, followed by interfacial electron transfer to adsorbed acceptor and donor molecules and ions. Thus, photoholes can be involved in the oxidation of organic substances, whereas ions of noble metals (Pd, Ag, etc.) and some transition metals having sufficiently positive electrochemical potential (e.g., Cu) can be reduced to their elemental forms by the photogenerated electrons [4–6]. The first reports on the possibility to use $TiO_2$ photolayers for the selective photocatalytic deposition yielding metal patterns appeared in the late 1960s [7–11] and the early results on the photopatterning utilizing titania-catalyzed photocatalytic reactions have been comprehensively reviewed [7,12,13].

Photoselective deposition of low resistivity metals (silver, copper) employing $TiO_2$-photolayers opens fresh opportunities for the production of large-area, high resolution flat panel displays such as liquid-crystal displays (LCD), plasma display panels (PDP), and electroluminescent displays (ELD) as well as different microelectronic devices [14–17]. In our previous papers [18,19], a new photopatterning process with the use of a photosensitive layer consisting of amorphous $TiO_2$ and water-soluble polyvinyl alcohol was proposed; this phototechnology permits generation of Ni–Cu patterns with thickness of 3–5 μm and resolution down to 10–12 μm.

The drawback of this technology is that the metal pattern generation cannot be performed on conducting substrates ($n^+$–Si, ITO, etc.) and requires deposition of an annealed $TiO_2$ layer, which is not easily removed from free areas after pattern generation. The aim of the present work was to investigate the possibility of photoselective metal deposition utilizing thin films of hydrated titanium oxide loaded with both sensitizing agents and metal ions capable of being reduced under UV irradiation and to clarify the mechanism underlying this photoprocess. Such a photolayer, which enables generation of catalytically active

* Corresponding author at: Display Device and Material Lab, Samsung Advanced Institute of Technology, P.O. Box 111, Suwon 440-600, Republic of Korea. Tel.: +82 31 280 6726; fax: +82 31 280 9349.
*E-mail addresses:* tamara.byk@samsung.com, tamara.byk@gmail.com (T.V. Byk).

1010-6030/$ – see front matter © 2007 Elsevier B.V. All rights reserved.
doi:10.1016/j.jphotochem.2007.06.007

metal centers in a single step, is favorable for the formation of microelectrodes on conducting substrates.

## 2. Experimental

The process of photoselective nickel deposition with a $Pd^{2+}$-loaded photosensitive layer of hydrated amorphous titanium oxide ($TiO_2$–$Pd^{2+}$ layer), which also contains oxalic acid as a chemical sensitizer, involves the following principle steps (Fig. 1):

(i) deposition of light-sensitive composite $TiO_2$–$Pd^{2+}$;
(ii) exposure of the resulted film with UV light through a quartz photomask;
(iii) washing with aqueous solution of 2-propanol permitting to dissolve titania on the unexposed areas;
(iv) nickel electroless plating.

By changing the irradiation intensity, it is possible to generate both negative (Fig. 1a) and positive nickel patterns (Fig. 1b).

$TiO_2$–$Pd^{2+}$ films (0.05 μm in thickness) were deposited onto conducting and nonconducting substrates (glass, pyroceramics, ITO glass, Si, ITO–polyethylenenaphthalate, etc.) from solution containing polybutyltitanate (0.5%), oxalic acid (0.5%), and $H_2PdCl_4$ (0.05%) in 2-propanol via spin-coating and used as photolayers without any additional treatments. The light of 350–1000 W mercury–xenon lamp was used for the UV exposure. Incident light intensity was varied from 8 (low intensity UV irradiation) to 30 mW $cm^{-2}$ (high intensity UV irradiation). The exposure time in all cases was set at 60 s. For washing of the exposed photolayers, a water/2-propanol mixture (10 vol.%) was used. A hypophosphite Ni electroless plating solution (Uyemura Co.) was employed to produce nickel patterns.

The X-ray diffraction patterns of the $TiO_2$–$Pd^{2+}$ layers were obtained with Cu Kα radiation using an X'pert-MFD diffractometer (Philips). FT-IR spectra were measured using an Equinox-55 FT-IR spectrometer (Bruker). X-ray photoelectron spectroscopic (XPS) measurements were performed on a Quantum 2000 Microprobe PHI spectrometer with a monochromatic Al Kα source and a charge neutralizer; all the binding energies were referenced to the C 1s peak at 284.5 eV of adventitious carbon. For comparison, the Pd 3d binding energies were also measured for $PdCl_2$, PdO and nanodispersed Pd which was deposited onto the $TiO_2$ film via photocatalytic reduction of $Pd^{2+}$. High resolution transmission electron microscopy (HRTEM) images were obtained using a $G^2$ FE-TEM microscope (Tecnai). To calculate the average size of palladium particles, the data on the diameter of 60 particles were used in each case. Surface roughness and morphologies of $TiO_2$–$Pd^{2+}$ films at different stages of development were

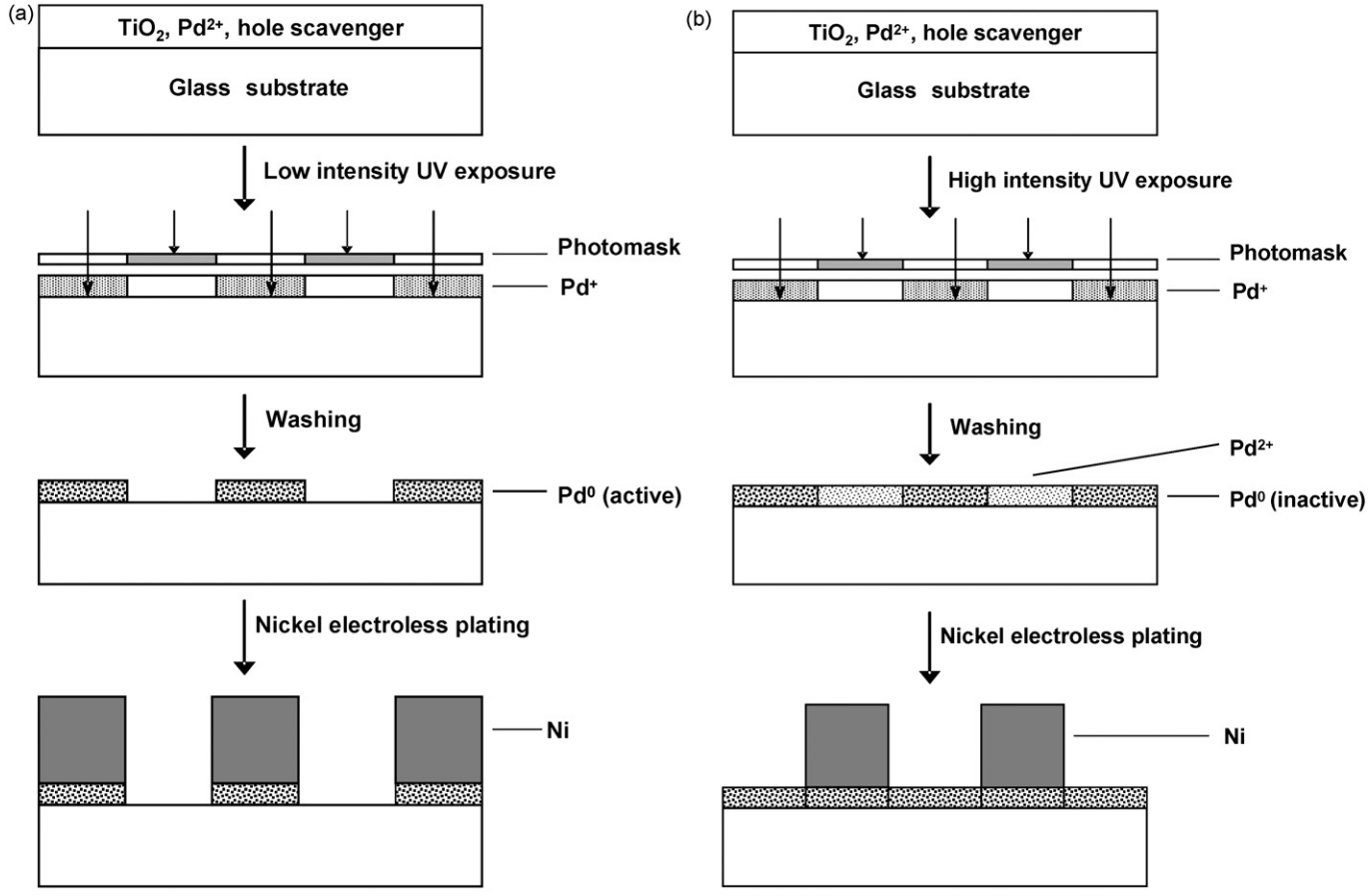


Fig. 1. Schematic diagram of nickel photopatterning process yielding: (a) negative pattern and (b) positive pattern. $Pd^0$ (active) and $Pd^0$ (inactive) are active palladium nanoparticles capable of inducing nickel electroless deposition and inactive palladium nanoparticles, respectively.

evaluated by AFM Dimension 3100 (Veeco Co.). Scanning electron microscopic observations were performed employing a SEM S-4700 (Hitachi). Photoelectrochemical measurements were carried out under potentiostatic conditions using the 365-nm line of a high-pressure Hg lamp (120 W) as the illumination source. As the working electrodes, the thin films of hydrated titanium oxide applied onto ITO glasses were used. Before photoelectrochemical measurements, the titania films were exposed to high intensity UV irradiation in order to photopolymerize the titania and to ensure its stability in aqueous media.

## 3. Results

### 3.1. X-ray diffraction from $TiO_2$–$Pd^{2+}$ photolayer

Fig. 2 shows the XRD pattern for $TiO_2$–$Pd^{2+}$ film. Only a wide peak is observed around $2\theta = 25^\circ$, which corresponds to the reflection from the anatase (1 0 1). No other reflections were detected, indicating that the titania film under investigation is amorphous.

### 3.2. X-ray photoelectron spectroscopy (XPS) studies

Figs. 3–6 show the Pd 3d and Ti 2p binding energy regions for $TiO_2$–$Pd^{2+}$ films, which were: (i) unexposed to UV irradiation; (ii) exposed to UV irradiation of different intensities; (iii) washed after exposure in the water/2-propanol (10 vol.%); or (iv) washed but not preliminary exposed. It is seen from Figs. 3 and 4 that the Pd $3d_{5/2}$ line for the first (i.e., unexposed to UV light) $TiO_2$–$Pd^{2+}$ film appears at *ca.* 336 eV, which coincides with the binding energy for Pd(II) in palladium oxide (336.4 eV) rather than in $PdCl_2$ (337.8 eV), though the chloride complex of palladium was used for photolayer preparation. Taking into account that the oxalic complex of palladium with $pK_1 = 8.7$ exhibits much higher stability as compared to the chloride complex ($pK_1 = 4.5$), it can be supposed that in the $TiO_2$–$Pd^{2+}$ film palladium ions are bound in the oxalic complexes. Figs. 3 and 4 (curve b) show that upon exposure to UV light, only a slight shift of palladium 3d electron peaks towards lower binding energies is observed. In case of $TiO_2$–$Pd^{2+}$ films exposed to high intensity UV light this shift is especially small and a shoulder to the lower-binding-energy side of the main peak arises, suggesting that

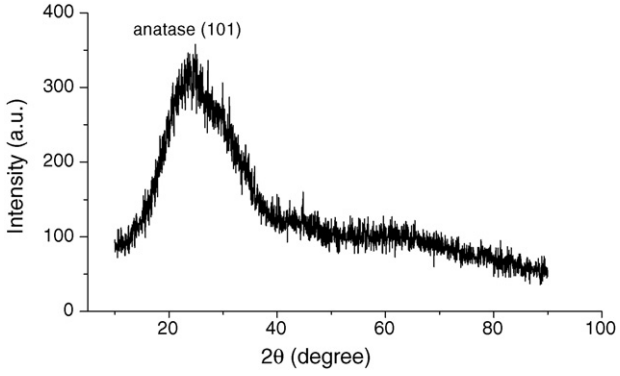


Fig. 2. X-ray diffraction pattern of $TiO_2$–$Pd^{2+}$ photolayer.

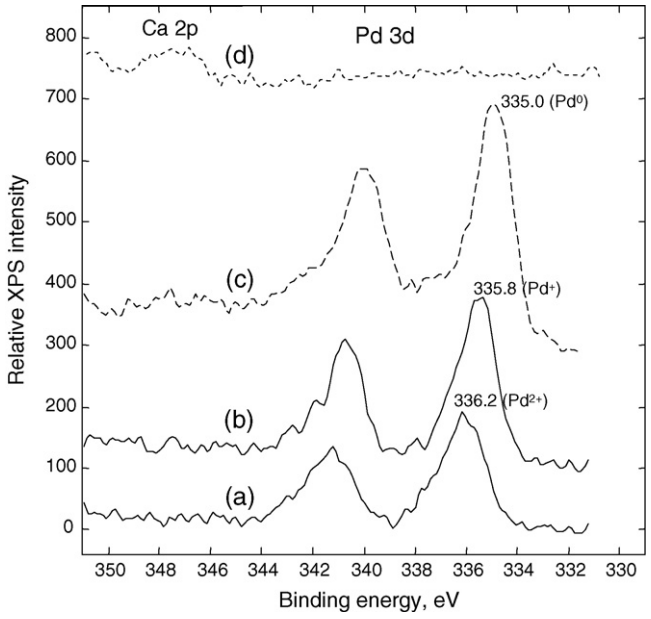


Fig. 3. X-ray photoelectron spectra of palladium in $TiO_2$–$Pd^{2+}$ photolayers: (a) unexposed to UV irradiation; (b) exposed to low intensity UV irradiation (~8 mW $cm^{-2}$); (c) exposed and washed; (d) not exposed but washed. Washing time: 1 min.

considerable amount of Pd(II) remains unreduced upon exposure. After washing (Figs. 3 and 4, curve c), the Pd $3d_{5/2}$ binding energy exhibits a further decrease, down to *ca.* 335 eV, reaching values characteristic of palladium nanoparticles deposited onto titania (334.9 eV). The Pd $3d_{5/2}$ binding energy for exposed $TiO_2$–$Pd^{2+}$ films thus lies between the values typical of Pd(II) and Pd(0), suggesting that Pd(II) exhibits photoreduction predominantly into Pd(I). This is consistent with the fact that the

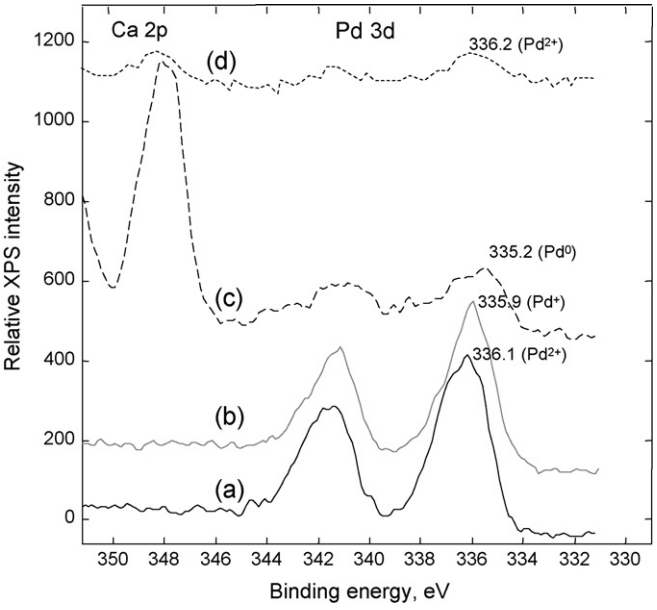


Fig. 4. X-ray photoelectron spectra of palladium in $TiO_2$–$Pd^{2+}$ photolayers: (a) unexposed to UV irradiation; (b) exposed to high intensity UV irradiation (~30 mW $cm^{-2}$); (c) exposed and washed; (d) not exposed but washed. Washing time: 10 s.

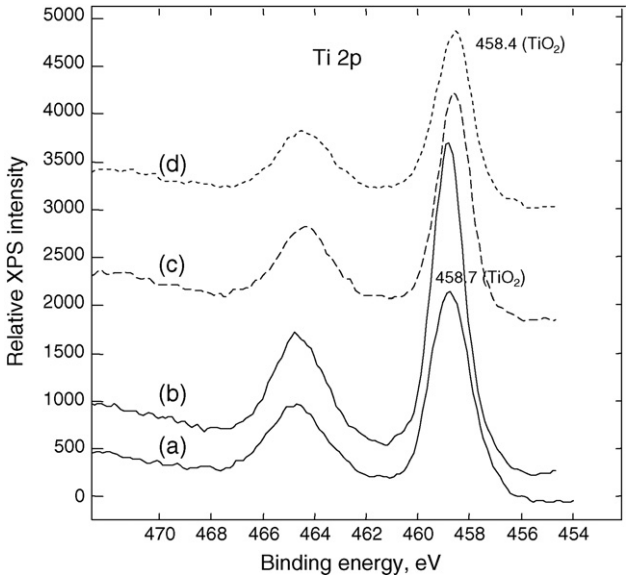


Fig. 5. X-ray photoelectron spectra of titanium in $TiO_2$–$Pd^{2+}$ photolayers: (a) unexposed to UV irradiation; (b) exposed to low intensity UV irradiation (~8 mW cm$^{-2}$); (c) exposed and washed; (d) not exposed but washed. Washing time: 1 min.

reduction of palladium complexes in the porous oxide matrixes under the mild conditions yields $Pd^{+}$ centers stabilized in the oxide host [20]. The Pd 3d photoelectron signal which is due to photoproduced palladium appears to be dependent on the intensity of UV illumination: the area of the Pd $3d_{5/2}$ photoelectron peak decreases by *ca*. five times when going from low intensity illumination to high intensity illumination. It is also seen from Figs. 3 and 4 that washing of unexposed $TiO_2$–$Pd^{2+}$ layers results in the efficient removal of $Pd^{2+}$: only traces of Pd(II) are observed in the photoelectron spectrum upon washing for 10 s

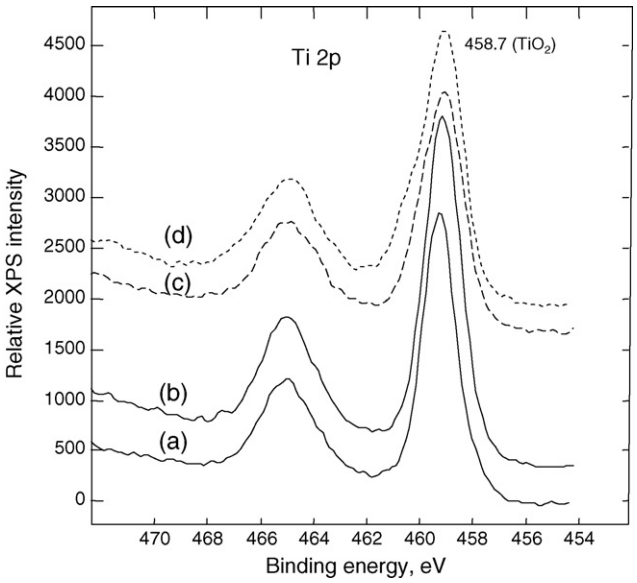


Fig. 6. X-ray photoelectron spectra of titanium in $TiO_2$–$Pd^{2+}$ photolayers: (a) unexposed to UV irradiation; (b) exposed to high intensity UV irradiation (~30 mW cm$^{-2}$); (c) exposed and washed; (d) not exposed but washed. Washing time: 10 s.

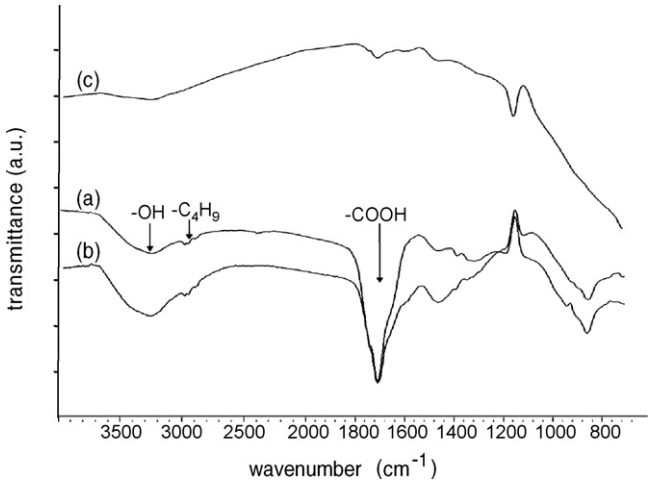


Fig. 7. FT-IR spectra of $TiO_2$–$Pd^{2+}$ photolayers (a) before and (b, c) after UV irradiation with intensity of: (b) 8; (c) 30 mW cm$^{-2}$.

(Fig. 4, curve d), whereas no signal from palladium is detected after 1 min washing (Fig. 3, curve d). After washing of unexposed $TiO_2$–$Pd^{2+}$ films and those exposed to UV irradiation, a calcium 2p electron peak arises in the photoelectron spectra. This peak can be attributed to the dissolution of the photolayer with the baring the glass substrate (curves c and d in Figs. 3 and 4).

The titanium 2p binding energies are characteristic of amorphous titania and show only a mere change with UV exposure and subsequent washing (Figs. 5 and 6). It should also be noted that the Ti 2p photoelectron signal exhibits gradual decrease during the course of washing of the unexposed $TiO_2$–$Pd^{2+}$ films but does not disappear completely. As a result, the pronounced Ti 2p peaks are observed in the photoelectron spectra (Figs. 5 and 6, curve d) providing evidence that dissolution of titania film during washing is incomplete.

### 3.3. FT-IR spectroscopy studies

In the FT-IR spectra for $TiO_2$–$Pd^{2+}$ photosensitive layers (Figs. 7 and 8) a pronounced band at ~1700 cm$^{-1}$ correspond-

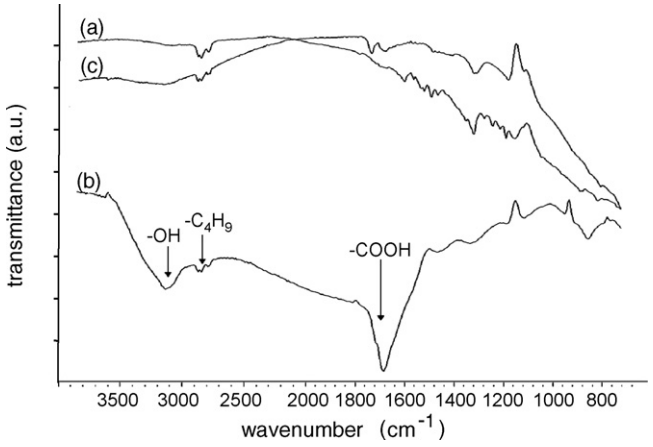


Fig. 8. FT-IR spectra of $TiO_2$–$Pd^{2+}$ photolayers: (a) after washing of unexposed sample; (b, c) after washing of samples exposed to UV light with intensity of: (b) 8; (c) 30 mW cm$^{-2}$.

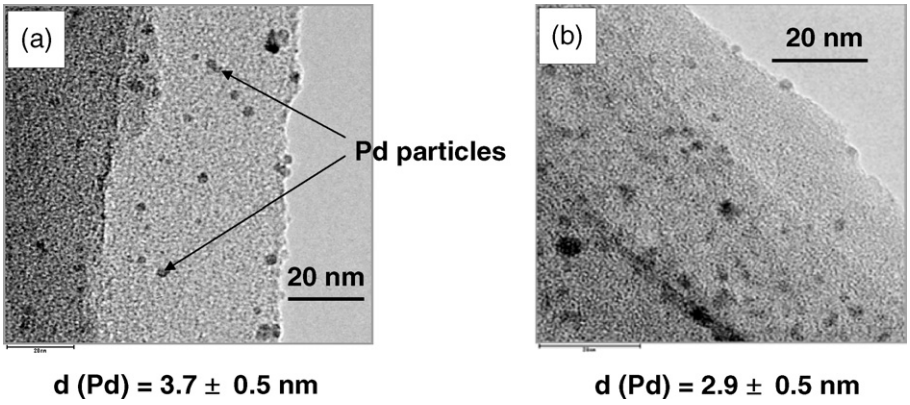


Fig. 9. Typical high resolution TEM images showing Pd particles generated by UV irradiation with intensity of: (a) 8; (b) 30 mW cm$^{-2}$.

ing to the carbonyl group of oxalic acid is observed. A weak band at *ca*. 2900 cm$^{-1}$ is related to stretching of butyl groups remaining in the titania upon hydrolysis, whereas IR bands positioned in the region of 3600–3100 cm$^{-1}$ can be assigned to the stretching of hydroxyl groups for oxalic acid as well as hydroxyls for dissociated and molecularly adsorbed water. With low intensity UV illumination, the IR band assigned to the stretching of the carbonyl group exhibits degradation due to consumption of oxalic acid in the photocatalytic process, while butyl groups in titania film remain almost untaken (Fig. 7, curve b). In contrast, the exposures to high intensity UV light results not only in almost complete oxidation of oxalic acid but also in degradation of hydroxyl groups and adsorbed water (Fig. 7, curve c). The disappearance of the IR band corresponding to the C=O groups observed after washing of unexposed $TiO_2$–$Pd^{2+}$ films (Fig. 8, curve a) indicates that oxalate has left the titania layer (together with Pd(II), as evidenced by XPS measurements—see above).

### 3.4. TEM analysis of UV-exposed photolayers

For TEM investigations, an aliquot of solution from which $TiO_2$–$Pd^{2+}$ films were derived was placed on a carbon coated copper grid and exposed to UV light. Spherical Pd particles with medium size of 3.7 ± 0.5 nm were obtained when low intensity irradiation was used (Fig. 9a). The Fourier filtrated and transformed (FFT) diffractogram [21] confirmed that these particles were crystalline. By contrast, the TEM images evidence that exposure with high intensity UV light leads to the formation of smaller Pd particles with medium size of 2.9 ± 0.5 nm (Fig. 9b). The FFT diffractograms of these particles show that they have amorphous structure. Our previous studies on the palladium nanophase produced via photolysis of palladium oxalate have revealed that only sufficiently large Pd particles (with a diameter of *ca*. 4 nm) with a pronounced degree of crystallinity are capable of catalyzing nickel deposition from an electroless plating bath employing hypophosphite as a reducing agent [22]. Pd particles of lower size exhibit dissolution during development in the nickel electroless plating solution [22].

### 3.5. Photoelectrochemical studies of the intrinsic photoactivity of hydrated titanium oxide

It is seen from Fig. 10 that thin films of amorphous titanium oxide can generate anodic photocurrent in a photoelectrochemical cell under negative bias. This demonstrates that titania derived at low temperatures possesses intrinsic photoactivity. However, the photoactivity of amorphous titania is about three times lower than that of polycrystalline $TiO_2$ films obtained by heating the film of amorphous titania at 450 °C.

### 3.6. SEM and AFM analyses of surface profile of the $TiO_2$–$Pd^{2+}$ films after their UV irradiation and washing

The SEM images shown in Fig. 11 evidence that washing of the $TiO_2$–$Pd^{2+}$ photolayer exposed through a photomask results in partial dissolution of titania at the unexposed areas yielding a rough surface. The detailed information on the changes in the surface morphology of $TiO_2$–$Pd^{2+}$ films at different steps of photopatterning process was gained from the AFM measurements. It is seen from 3D images obtained with AFM that the roughness of titania film exhibits an increase upon exposure (Fig. 12):

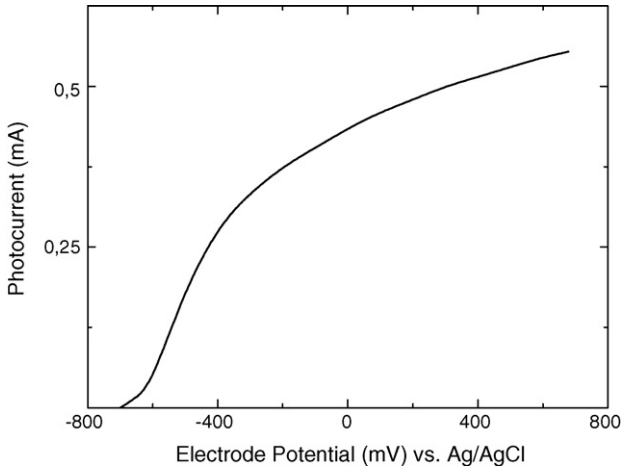


Fig. 10. Photocurrent vs. potential dependence for $TiO_2$–$Pd^{2+}$/ITO electrode under UV illumination. Electrolyte: 0.25 M $NaSO_4$.

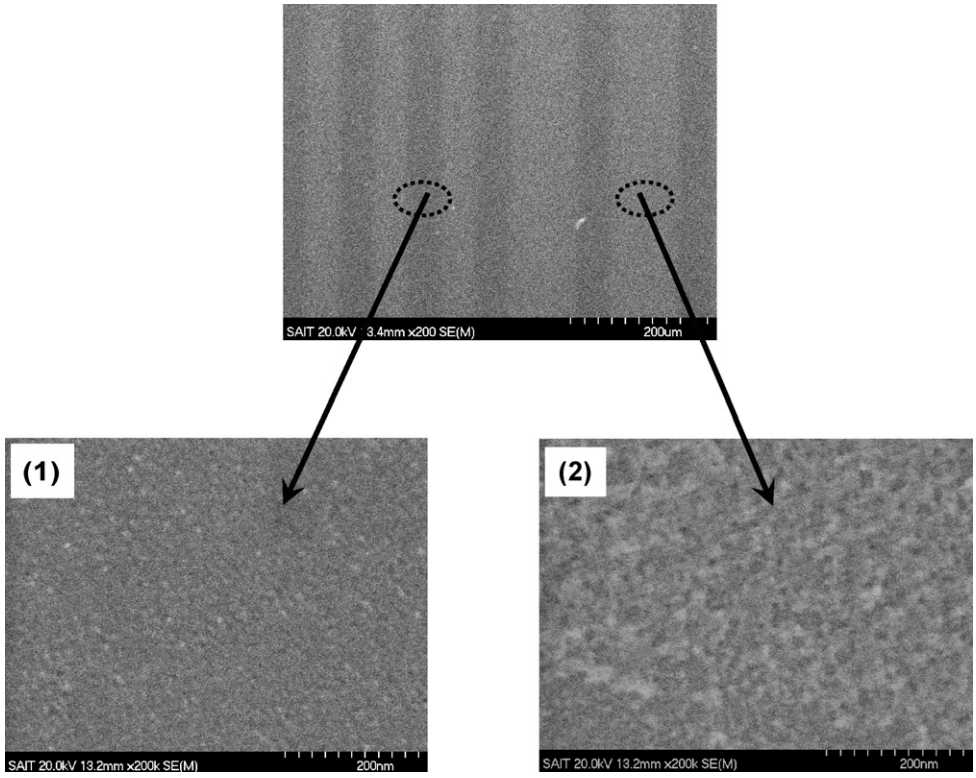


Fig. 11. SEM image of $TiO_2$–$Pd^{2+}$ photolayer irradiated through a quartz photomask with UV light (8 mW cm$^{-2}$) and then washed: (1) exposed area and (2) unexposed area.

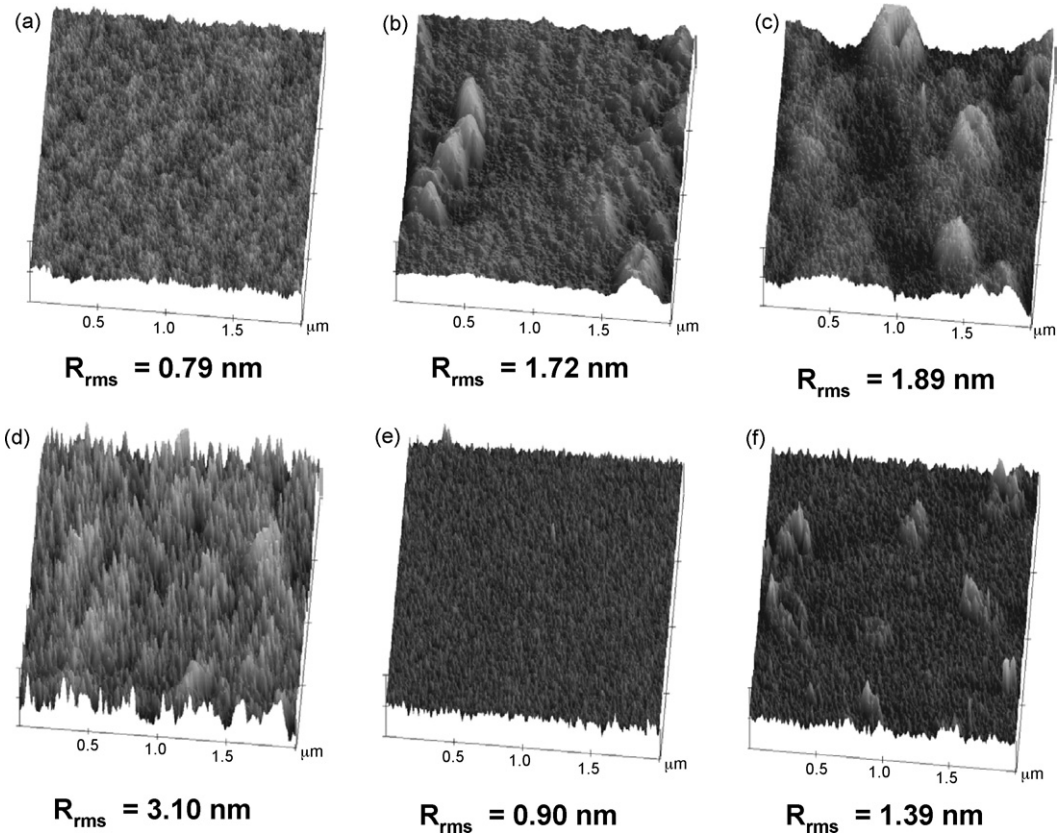


Fig. 12. AFM 3D images of $TiO_2$–$Pd^{2+}$ photolayers: (a) unexposed; (b, c) exposed to UV irradiation; (d) washed but not exposed; (e, f) exposed and washed. UV irradiation intensity: (b, e) 8 mW cm$^{-2}$; (c, f) 30 mW cm$^{-2}$.

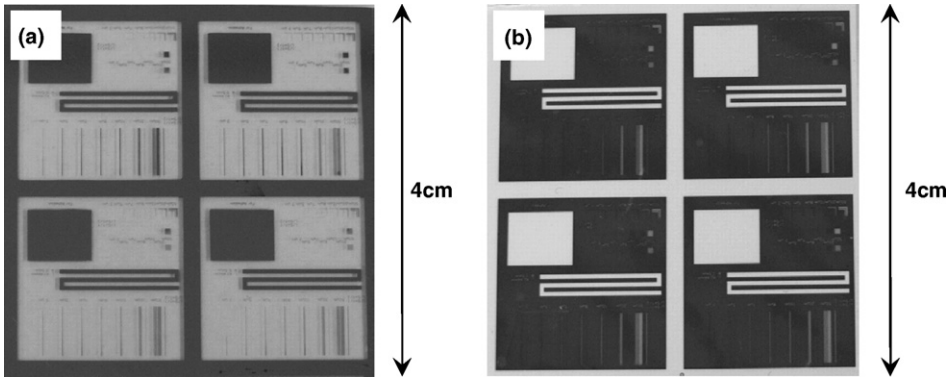


Fig. 13. Photoimages of nickel patterns of (a) negative type and (b) positive type obtained on glass substrates. Time of nickel electroless plating: (a) 1; (b) 3 min. Washing time: (a) 1 min; (b) 10 s.

the root mean square roughness ($R_{rms}$) increases from an initial value of 0.79 to 1.72–1.89 nm. After washing, the surface of the pre-exposed film becomes smoother (the surface roughness falls to 0.9 nm for $TiO_2$–$Pd^{2+}$ films exposed to low intensity UV light and to 1.39 nm for those exposed to high intensity UV light), whereas the titania particles remaining at the unexposed areas after washing are responsible for high roughness of the resulting surface ($R_{rms}$ = 3.10 nm).

### 3.7. Photopatterning with the use of $TiO_2$–$Pd^{2+}$ films

The UV exposure of $TiO_2$–$Pd^{2+}$ films deposited onto a glass substrate was carried out through a negative type quartz photomask. Depending on the UV light, both negative and positive metal patterns can be generated (Fig. 13). To obtain negative metal patterns (nickel deposition occurs at the exposed areas), photolayers were exposed to low intensity UV light (~8 mW $cm^{-2}$) followed by washing in water/2-propanol mixture (10 vol.%) for 1 min and then in the distilled water for 1–2 min. The time of nickel electroless plating over the photoproduced Pd centers was about 1 min, which yields Ni layers ~0.1 μm in thickness. In contrast, to generate positive metal patterns (nickel deposition occurs at the unexposed areas), $TiO_2$–$Pd^{2+}$ photolayers were irradiated with high intensity UV light (~30 mW $cm^{-2}$). Thus exposed photolayers were washed in water/2-propanol mixture (10 vol.%) for only 10 s and then rinsed with distilled water, whereas the electroless nickel deposition time was about 3 min. The thickness of the resultant Ni layer was of ~0.2 μm.

## 4. Discussion

The photodeposition process is initiated when light with energy larger than the amorphous $TiO_2$ bandgap (3.92 eV [18,19]) is absorbed by titania, forming an electron–hole pairs, as illustrated by the following equation:

$$TiO_2 + h\nu \rightarrow e^-_{CB} + h^+_{VB} \quad (1)$$

here the subscripts CB and VB denote the conduction and valence bands, respectively.

In amorphous titania, the photoelectrons and photoholes are separated mainly owing to interfacial reactions. The XPS studies (Figs. 3 and 4) indicate that $Pd^{2+}$ ions during exposure exhibit reduction predominantly to Pd(I) compounds stabilized in the titania matrix. At the washing stage, when the exposed film is in contact with water, the photoproduced Pd(I) centers exhibit conversion into palladium nanophase through disproportionation as in the following equation

$$2Pd(I) \rightarrow Pd + Pd(II) \quad (2)$$

The palladium ions produced via this reaction, together with Pd(II) at the unexposed areas, leave the photolayer in solution during washing. Simultaneously the titania on the unexposed areas dissolves. Notwithstanding the fact that the dissolution of the oxide film is incomplete and fine titania particles remain on the unexposed areas yielding rather rough surface, the thorough washing in water/2-propanol mixture and then in distilled water ensures complete removal of Pd(II) as evidenced by XPS measurements (Figs. 3 and 4).

The photoholes produced under illumination are effectively trapped via the reaction of irreversible oxidation of oxalate as in the following equation

$$2h^+ + C_2O_4{}^{2-} \rightarrow 2CO_2 \quad (3)$$

However, at high exposure doses, when oxalate appears to be consumed to a large extent (as evidenced by degradation of the IR band at 1700 $cm^{-1}$ corresponding to vibrations of the C=O group, Fig. 7) the photoholes begin to oxidize Pd(I). This "short circuit" effect results in a lower amount of $Pd^0$ remaining in the titania layer upon exposure (*cf.* curve c in Figs. 3 and 4).

The surface hydroxyl groups and water molecules trapped in titania film compete with oxalate for photoholes, as shown by the following equations:

$$Ti\text{–}OH + h^+ \rightarrow Ti\text{–}^{\bullet}OH \quad (4)$$

$$H_2O + h^+ \rightarrow {}^{\bullet}OH + H^+ \quad (5)$$

yielding * OH radicals radicals which can also be involved in the oxalate oxidation. On the other hand, oxidation of the $TiO_2$ surface groups by photogenerated holes results in further polymerization of hydrated titania through the formation of oxygen

bridges, as illustrated by the following equation

$$2\text{Ti–OH} + 2h^+ \rightarrow \text{–Ti–O–Ti–} + H_2O \quad (6)$$

As a result, inner strains arise in the titania film, which manifest themselves in a profound increase in the surface roughness upon exposure; washing of the exposed film is accompanied by further rearrangements, resulting in a smoother surface (Fig. 12). Due to photopolymerization, the solubility of the exposed titanium films exhibits a drastic decrease as compared with unexposed ones. These observations agree well with previous results [13], showing that the UV light-induced polymerization of hydrated $TiO_2$ films enhances the compactness of the film (the film thickness decreases *ca*. twofold upon UV irradiation) and drastically reduces its solubility. However, the enhanced Ca 2p peak observed in the photoelectron spectrum for $TiO_2$–$Pd^{2+}$ film exposed to high intensity UV light and then washed (Fig. 4, curve c) permits a conclusion that titania photolayer after profound photopolymerization loses its adhesion and partially degrades during washing stage yielding an islet film. This degradation of titania film may also be responsible for low concentration of palladium remaining at the exposed areas upon washing.

The photopolymerization of $TiO_2$–$Pd^{2+}$ films under UV light yields dense titania matrix providing a confined medium for metal nanophase formation. Due to the differences in the structure of the titania host and $Pd^0$ yield in the cases of samples exposed with low intensity and high intensity UV light, palladium particles that differ in structure and dispersity are formed. Meanwhile, exposure to low intensity UV light produces crystalline Pd particles with medium size close to the critical size for nickel electroless plating (*ca*. 4 nm) and exposure to high intensity UV light yields much smaller particles of amorphous palladium. In the former case, Pd nanoparticles exhibit high catalytic activity towards nickel deposition, which enables generation of negative nickel patterns (Fig. 13a). In contrast, palladium particles produced as a result of high intensity illumination appear to be catalytically inactive and fail to induce nickel deposition at the exposed areas. On the other hand, $Pd^{2+}$ remaining on the unexposed areas after brief washing can be reduced during prolonged treatment in the nickel hypophosphite electroless plating bath, yielding catalytic Pd centers that can ensure nickel deposition on the unexposed areas. This results in the formation of a nickel positive pattern (Fig. 13b). Similar switching of the photopatterning process from a negative to a positive one was demonstrated previously for overexposed photosensitive layers based on thin films of polyvinyl alcohol loaded with $PdCl_2$ and $Fe_2(C_2O_4)_3$ [23]; this switching was, however, attributed to the formation at high exposure doses of large Pd particles exhibiting low catalytic activity. In the case of $TiO_2$–$Pd^{2+}$ photolayers, a different mechanism of photopatterning switching is realized, which is due to the photooxidation of a latent image when the hole scavengers are exhausted and to the formation of palladium nanoparticles of poor crystallinity in the photopolymerized titania matrix.

## 5. Conclusions

The mechanism of photoselective nickel deposition with the use of thin films of amorphous titanium dioxide loaded with $Pd^{2+}$ and oxalic acid as a hole scavenger has been investigated.

Under UV irradiation, photoreduction of $Pd^{2+}$ residing in the photolayer in the form of an oxalic complex occurs predominantly as a one-electron reaction yielding Pd(I) compound stabilized in the titania matrix, while the oxalic acid and surface hydroxyl groups of hydrated amorphous $TiO_2$ are oxidized by photoholes. Actinic illumination is also accompanied with photopolymerization of hydrated titania, leading to profound losses in solubility of the photolayer at exposed areas. Washing results in the removal of the photolayer from the unexposed areas. However, this removal is incomplete and leads to high roughness of the resultant surface. Washing also facilitates the formation of a Pd nanophase at UV-exposed areas via a disproportionation mechanism, the structure and dispersity of these Pd particles being dependent on the intensity of UV irradiation. Pd particles of crystalline structure and a size of *ca*. 4 nm produced upon low intensity UV irradiation can catalyze the subsequent Ni electroless deposition, providing a negative metal pattern formation. On the other hand, amorphous Pd particles of smaller size produced upon high intensity illumination do not possess catalytic activity. Pd(II) remaining at the unexposed areas upon brief washing is, however, capable of inducing nickel electroless deposition with the formation of a metal pattern of positive type. This opens the possibility of straightforward switching of the photopatterning process by changing the illumination intensity.

## References

[1] A. Fujishima, T.N. Rao, D.A. Truk, J. Photochem. Photobiol. C: Photochem. Rev. 1 (2000) 1.
[2] M.R. Hoffmann, S.T. Martin, W. Choi, D.W. Bahnemann, Chem. Rev. 95 (1995) 69.
[3] E. Kaneko, I. Okura, Photocatalysis: Science and Technology, Springer, Berlin, 2002.
[4] A. Hilmi, J.H.T. Luong, A.L. Nguyen, Chemosphere 38 (1999) 865.
[5] M.I. Litter, Appl. Catal. B 23 (1999) 89.
[6] D.G. Shchukin, E.A. Ustinovich, D.V. Sviridov, Yu.M. Lvov, G.B. Sukhorukov, Photochem. Photobiol. Sci. 2 (2003) 975.
[7] V.V. Sviridov, in: A.L. Kartuzhanskii (Ed.), Nonsilver Photographic Processes (in Russian), Khimiya, Leningrad, 1984, pp. 242–307.
[8] H. Jonker, C.J. Dippel, H.J. Houtman, et al., Photogr. Sci. Eng. 13 (1969) 1.
[9] H. Jonker, C.J. Janssen, C.J. Dippel, et al., Photogr. Sci. Eng. 13 (1969) 45.
[10] E. Berman, Photogr. Sci. Eng. 13 (1969) 50.
[11] G.L. McLeod, Photogr. Sci. Eng. 13 (1969) 93.
[12] V.V. Sviridov, V.G. Sokolov, G.A. Branitskii, Signal AM 12 (1984) 211.
[13] Yu.V. Nechepurenko, V.G. Sokolov, Sci. Appl. Photo. 35 (1994) 765.
[14] J. Rickerby, J.H. Steinke, Chem. Rev. 102 (2002) 1525.
[15] G.S. Chae, G.C. Jo, US Patent 6515726 (2003).
[16] J. Tate, J.A. Rogers, C.D.W. Jones, et al., Langmuir 16 (2000) 6054.
[17] S.W. Lee, B.K. Choo, D.Y. Kim, K.S. Cho, J. Jang, Proceedings of the SID 02 DIGEST, 2002, p. 916.
[18] C.H. Noh, J.Y. Kim, O.C. Hwang, S.H. Cho, K.Y. Song, T.V. Byk, V.G. Sokolov, T.V. Gaevskaya, J.B. Kim, Electrochem. Solid-State Lett. 8 (2005) 1.

[19] C.H. Noh, J.Y. Kim, O.C. Hwang, S.H. Cho, K.Y. Song, T.V. Byk, V.G. Sokolov, J.B. Kim, Chem. Lett. 34 (2005) 82.
[20] A.Yu. Stakheev, O.P. Tkachenko, Russ. J. Phys. Chem. 72 (1998) 1925.
[21] D.B. Williams, C.B. Carter, Transmission Electron Microscopy "A Textbook for Materials Science", Plenum Press, New York, 1996.
[22] V.V. Sviridov, T.N. Vorob'eva, T.V. Gaevskaya, L.I. Stepanova, Chemical Deposition of Metals from Aqueous Solutions, Universitetskoje Publ., Minsk, 1987 (in Russian).
[23] S.N. Malchenko, V.V. Sviridov, Z.L. Petrushkina, Z.I. Lubimova, Zh. Nauch. i Prikl. Foto. i Kinematografii 22 (1977) 241.